Proteomics Analysis of the Protective Effects of Hesperetin on Coronary Artery injury in Streptozotocin-Induced Type 1 Diabetic Rats

Guofang Xing
ShanXi Medical University
Pingting Huo
Shanxi Medical University
Xinyi Zhang
Shanxi Medical University
Zhaoyang Chen
Shanxi Medical University
Lei Wang
Shanxi Medical University
Yu Liu (hitec@126.com)
Shanxi Medical University https://orcid.org/0000-0003-2004-4900

Research

Keywords: cardiovascular disease, diabetes, hesperetin, proteomics, Toll-like receptor binding

Posted Date: December 10th, 2020

DOI: https://doi.org/10.21203/rs.3.rs-122889/v1

Abstract

Background: Type 1 and type 2 diabetes both cause damage to the cardiovascular system. Hesperetin, a medicinal product found in foods, has been shown to have various cardioprotective effects. However, the effects of this compound on diabetes-related cardiovascular damage have not been evaluated.

Methods: In this study, we aimed to investigate the protective effects of hesperetin on the coronary artery in diabetic rats and to explore its effects on the changes in critical proteins in the coronary artery using proteomics analysis.

Results: Hesperetin alleviated coronary artery injury and modulated the expression of various proteins, including S100A8 and S100A9, which functioned in Toll-like receptor 4 binding, Toll-like receptor binding, and RAGE receptor binding. Pathways altered by hesperetin included type I diabetes mellitus, cell adhesion molecules, antigen processing and presentation, and interleukin-17 signaling pathway.

Conclusions: In this study, we constructed a protein map of SD rats with type 1 diabetes treated with hesperetin, and found significant changes in three important proteins, S100A8, S100A9 and KNG1.Our findings provided important insights into further studies of the cardiovascular protective effects of hesperetin.

Introduction

Diabetes is a common endocrine metabolic disease. The prevalence of diabetes has increased rapidly in the last 3 years, making diabetes one of the most common non-communicable diseases worldwide. According to the ninth edition of the Diabetes Atlas released by the International Diabetes Federation in 2019, the global prevalence of diabetes is expected to increase to 10.2% (578 million) by 2030 and 10.9% (700 million) by 2045 [1]. Although type 1 diabetes mellitus (T1DM) accounts for only a small proportion of the total number of cases, its incidence is also increasing [1]. Compared to the general population, patients with T1DM have a 10-fold increased risk of cardiovascular disease [2–5] and coronary artery disease is the leading cause of death in patients with T1DM [1, 2, 6].

The complex physiological changes associated with T1DM, including hyperglycemia [7], dyslipidemia [8], inflammation [9, 10], and oxidative stress [10, 11] adversely affect the cardiovascular system, leading to cardiovascular complications. The general treatment strategy involves lifestyle changes, insulin therapy, regular exercise, and glycemic control, as well as administration of hypoglycemic, lipid-lowering, and antihypertensive agents. However, the risk of cardiovascular events and death in patients with T1DM is still significantly higher than that in the general population [12]. Therefore, safer and more effective early interventions are needed to prevent T1DM-related cardiovascular diseases.

Hesperetin (Hst) is a natural flavonoid drug candidate that is abundant in food sources, including the citrus fruits of the Rutaceae family. Hst is mainly derived from the hydrolysis of hesperidin and has multiple biological and pharmacological functions. These flavonoids can exert antihyperglycemic [13],

anti-oxidation [14, 15], antihyperlipidemic [13], anti-atherosclerosis [16], and anti-inflammatory effects [17]. Moreover, the daily dietary intake of flavonoids is associated with a reduction in the incidence of cardiovascular diseases [18, 19]. For example, Hst has direct vasorelaxant effects on coronary arteries via the inhibition of L-type voltage-gated Ca^{2+} channels and the enhancement of voltage-gated K^{+} channel currents in myocytes [20]. Moreover, Hst effectively inhibits collagen and arachidonic acid-induced platelet aggregation by blocking phospholipase Cγ2 phosphorylation and cyclooxygenase-1 activity [21]. However, few studies have examined the mechanisms of Hst in the coronary artery.

Accordingly, in this study, we aimed to evaluate the protective effects of Hst on coronary artery injury in T1DM model rats. Because of difficulties in comprehensively exploring the mechanisms of Hst using traditional molecular biology methods, we used proteomics to screen and analyze differentially expressed proteins and identify proteins that are critical to mediating the effects of Hst on coronary artery injury in T1DM model rats. Our findings may establish novel targets for the development of drugs for the prevention and treatment of diabetic vascular disease.

Materials And Methods

Animals and groups

Healthy male Sprague-Dawley (SD) rats (license number: SCXK2009-001) weighing 220–280 g were provided by the Laboratory Animal Center of Shanxi Medical University. The animals were housed in separate cages at a room temperature of 20–25°C and relative humidity of 50–65% under a 12-h light-dark cycle and given free access to water and food. In total, 50 SD rats were divided into control (n = 14) and model groups (n = 36); seven rats died during the modeling process. After successful modeling, rats were randomly divided into the T1DM group (n = 14) and Hst group (n = 15). All animal experimental procedures complied with the Experimental Animal Ethics Committee of Shanxi Medical University.

Drug treatment

After fasting for 12 h, all rats, except those in the control group, were intraperitoneally injected with 1% streptozotocin (STZ; Sigma, USA) dissolved in citrate buffer (pH 4.2–4.5) at a dose of 65 mg/kg. Control rats were injected with the same volume of citrate buffer. After 3 days, blood glucose was measured via the tail vein, and rats with a blood glucose level exceeding 16.7 mM for more than 1 week were considered as having T1DM. Rats in the Hst group were then intragastrically administered 100 mg/kg/day Hst (Sigma) dispersed in 0.1% sodium carboxymethyl cellulose for 4 weeks, starting at 2 weeks after the STZ injection. The control and T1DM groups were intragastrically administered an equal amount of 0.1% sodium carboxymethylcellulose.

Hematoxylin and eosin (HE) staining

At the end of the experiment, rats in each group were anesthetized, their chest was opened, and the heart was removed and placed into a beaker containing PSS (pH 7.4) solution in an environment saturated with

a 95% O_2 and 5% CO_2 mixture at 4°C. After routine treatment, the hearts of three rats in each group were stained using HE dye solution (Servicebio, China), observed using microscopy (DM2500; Leica, Germany), and photographed using Leica Application Suite X software (LAS X).

Preparation of proteomic vascular samples

The hearts were removed from the beaker and fixed in a Petri dish with pins. After finding the coronary arteries using an anatomical microscope (Phenix, China), they were separated by carefully removing the muscle tissue around the blood vessels using surgical microscissors and forceps. The vascular specimens were placed in a cryotube, rapidly frozen in liquid nitrogen, and stored in a freezer at -80°C.

TMT-labeled quantitative proteomics

Protein sample preparation

Vascular samples were ground into a powder in liquid nitrogen and transferred to a 5-mL centrifuge tube. Then, four volumes of lysis buffer (8 M urea, 1% protease inhibitor, 3 μM TSA, 50 mM NAM) was added to the cell powder, followed by sonication three times on ice using a high-intensity ultrasonic processor (Scientz, China). After centrifugation at 4°C and 12000 × *g* for 10 min, the supernatants were collected, and the protein concentration was determined using a BCA kit (Beyotime, China).

Trypsin digestion

For digestion, the protein solution was reduced with 5 mM dithiothreitol for 30 min at 56°C and alkylated with 11 mM iodoacetamide for 15 min at 25±2 ℃in the dark. The urea concentration of the protein sample was diluted to less than 2 M. Trypsin was added at a mass ratio of 1:50 and 1:100 (trypsin:protein) for the first digestion overnight at 37°C and the second 4-h digestion, respectively.

TMT labeling

After trypsin digestion, peptides were desalted using a StrataXC18 SPE column (Phenomenex) and freeze-dried in a vacuum. Peptides were dissolved in 0.5 M TEAB and labeled with a TMT kit (Thermo, USA) according to the manufacturer's instructions. Briefly, the labeled reagent was thawed and dissolved in acetonitrile, mixed with peptides, and incubated at room temperature for 2 h. The peptide mixtures were pooled, desalted, and freeze-dried in vacuum. Three technical replicates were carried out per sample, and the samples were labeled as follows: control group, 126, 127C, 128N; T1DM group, 128C, 129N, 129C; Hst group, 130N, 130C, 131.

Fractionation using high-performance liquid chromatography (HPLC)

The peptides were fractionated using high pH reverse-phase HPLC using an Agilent 300Extend C18 column (5 μm particles, 4.6 mm ID, 250 mm length). Briefly, peptides were first separated using a gradient

of 8–32% acetonitrile (pH 9.0) over 60 min into 60 fractions. Then, the peptides were combined into nine fractions and freeze-dried in vacuum.

Liquid chromatography-tandem mass spectrometry (LC-MS/MS) analysis

The peptides were dissolved with LC mobile phase A (0.1% formic acid and 2% acetonitrile) and directly loaded onto a reversed-phase column (15 cm length, 75 μm ID). The gradient comprised an increase from 8% to 20% mobile phase B (0.1% formic acid and 90% acetonitrile) over 50 min, 20% to 35% in 35 min, and increasing to 80% in 3 min, then held at 80% for the last 3 min, all at a constant flow rate of 400 nL/min using an EASY-nLC 1000 UPLC system.

After separation using an ultra-high-performance liquid phase system, the peptides were injected into the NSI ion source for ionization and then analyzed using Orbitrap Fusion Lumos MS. The applied ion source voltage was 2.0 kV, and the scan range of the first-level MS was set to m/z 350–1550 with 60,000 resolution; the second-level MS was set to m/z 100 with 30,000 resolution. To improve effective utilization of the mass spectrum, the automatic gain control was set at 5E4, the signal threshold was 50000 ions/s, the maximum injection time was 70 ms, and the dynamic exclusion time of the tandem MS scan was 30 s to avoid repeated scanning of the peptide precursors.

Database search

LC-MS/MS raw data were processed from the UniProt Rattus database concatenated with a reverse decoy database and a common pollution database using Maxquant (v.1.5.2.8). The parameters were set as follows: algorithm, trypsin; maximum missed cleavages, 2; minimum peptide length, 7 amino acid residues; maximum modification number, 5. The mass error tolerance values of the precursors in the first and main search were 20 and 5 ppm, respectively, and the second fragment tolerance was 0.02 Da. Carbamidomethyl on Cys was specified as a fixed modification. Variable modifications were oxidation on Met and N-terminal acetylation of protein. The quantification type was TMT-10plex. The false discovery rate was set to 1%.

Bioinformatics methods

Gene Ontology (GO) annotations

The GO annotation proteome was derived from the UniProt-GOA database (https://www.ebi.ac.uk/GOA/). First, we converted the identified protein IDs to UniProt IDs and then mapped the proteins to GO IDs. If some identified proteins were not annotated by the UniProt-GOA database, InterProScan software was used to annotate the functions of the proteins based on the protein sequence alignment method. Then, proteins were classified into biological process, cellular component, and molecular function categories. For each category, two-tailed Fisher's exact tests were used to evaluate the enrichment of differentially expressed proteins. GO categories with corrected p values < 0.05 were considered significant.

Kyoto Encyclopedia of Genes and Genomes (KEGG) pathway annotation

The KEGG (https://www.genome.jp/kegg/pathway.html) database was used to annotate protein pathways. First, the KEGG online service tool KAAS was used to annotate protein, followed by mapping the annotation result of the KEGG pathway database using KEGG online service tools and KEGG mapper. Wolfpsort (https://www.genscript.com/psort/wolf_psort.html) was used to predict subcellular localization. For domain annotation, the identified protein domain functional descriptions were annotated using InterProScan and the InterPro domain database (http://www.ebi.ac.uk/interpro/), which integrates diverse information about protein families, domains, and functional sites. Lastly, the KEGG database was used to identify enriched pathways using two-tailed Fisher's exact tests. KEGG pathways with corrected p values of less than 0.05 were considered significant.

Protein-protein interaction network

All differentially expressed protein database accessions or sequences were searched against the STRING database (v. 11.0) for protein-protein interactions.

Western blot analysis

Coronary artery tissues of rats were ground in RIPA lysis buffer and protease inhibitor (phenylmethylsulfonyl fluoride) using an MP FastPrep-24 5G rapid sample preparation instrument (MP, USA). The precipitate was gently shaken for 30 min on a shaker and removed by centrifugation for 20 min at 4°C and 13000 × *g*, and the protein concentration was determined using a BCA kit (Boster, China). The samples were diluted to the same concentration, mixed with 5× loading buffer, boiled at 100°C for 5 min, cooled to room temperature, and stored at -20°C until use. The proteins were then separated using sodium dodecyl sulfate-polyacrylamide gel electrophoresis on 12% gels and transferred to polyvinylidene difluoride membranes. The membranes were blocked at room temperature for 2 h with 5% skim milk dissolved in TBST, washed with TBST three times for 10 min each, and incubated with the following antibodies overnight on a shaker at 4℃: anti-β-actin (1:5000 dilution; Bioworld, China), anti-Kng1 (1:1000 dilution; ABclonal, China), anti-S100A9 (1:1000 dilution; ABclonal), and anti-S100A8 (1:1000 dilution; ABclonal). The membranes were washed three times with TBST for 10 min each and incubated with horseradish peroxidase-labeled goat anti-rabbit IgG (1:10000 dilution; Boster) on a shaker at room temperature for 1 h. After washing the membranes with TBST, an appropriate amount of ultra-sensitive ECL Ready-to-use Substrate (Boster) was added, and the membranes were exposed to a ChemiDoc MP Imaging System (Bio-Rad Laboratories, USA).

Statistical analysis

Statistical analysis was performed using SPSS software (version 26.0). The results were compared using a one-way analysis of variance followed by least significant difference post-hoc tests. All data are expressed as means ± standard deviations and $P < 0.05$ was considered statistically significant.

Results

Hst attenuated STZ-induced weight loss and hyperglycemia in T1DM model rats

At the end of the experiment, body weight was significantly reduced in T1DM rats compared to control rats (Fig. 1a), whereas blood glucose was markedly increased (Fig. 1b). Treatment with Hst for 4 weeks attenuated weight loss and hyperglycemia in STZ-induced T1DM rats (Fig. 1a, b).

Histological examination of the coronary artery in rats

To evaluate the efficacy of Hst in the histology of the coronary artery under STZ-induced conditions, we used HE staining to examine the morphological structure of the rat coronary artery. The coronary arteries of control rats were clearly stratified; the intima was smooth and flat, and the vessel wall was not thickened (Fig. 2a). In contrast, the coronary arteries of STZ-induced T1DM rats showed a disordered arrangement of endothelial cells, proliferated smooth muscle cells, thickened vessel walls, and narrowed lumen (Fig. 2b). After Hst treatment, the coronary artery wall was thickened, but pathological changes in STZ-induced rats were alleviated (Fig. 2c).

Analysis of differentially expressed proteins using TMT

In order to further explore the critical proteins involved in mediating the effects of Hst on the coronary artery in T1DM rats, we analyzed differentially expressed proteins using TMT. Peptides digested by trypsin were analyzed using high-resolution MS, and the data were evaluated using various known bioinformatics databases. Most peptides contained 7–20 amino acids, consistent with trypsin enzymatic hydrolysis and HCD fragmentation (Fig. 3a). Theoretically, proteins with higher molecular weights can produce more enzymatic fragments, and more peptides need to be identified from a large protein to achieve the same coverage. The lengths of the identified peptides met the requirements for quality control (Fig. 3b). We used principal component analysis to evaluate the quantitative repeatability of protein identification. Closer clusters of repeated samples indicated better quantitative repeatability (Fig. 3c). When the p value was less than 0.05, changes in differential expression exceeded 1.2 as the threshold for significant upregulation or less than 1/1.2 as the threshold for significant downregulation (Fig. 3d).

Functional classification of the differentially expressed proteins in Hst/T1DM

To further characterize the identified proteins, we annotated the functions and characteristics of differentially expressed proteins in the Hst/TIDM group using multi-omics analysis databases. As shown in Fig. 4a, most differentially expressed proteins after hesperetin intervention were categorized in the biological process (BP) category, including single-organism processes (15%), cellular processes (14%), metabolic processes (13%), biological regulation (13%), response to stimulus (11%), and immune system (3%). The differentially expressed proteins were also categorized into the molecular functions (MFs; Fig. 4b) of binding (57%), catalytic activity (22%), molecular function regulator (8%), and transporter activity (6%). Similarly, the differentially expressed proteins belonged to cell (28%), organelle (25%), macromolecular complex (16%), extracellular region (10%), and membrane (9%) subcategories of the cell component (CC) category (Fig. 4c).

Wolfpsort was used to analyze the subcellular localization of differentially expressed proteins. As shown in Fig. 4d, among the 69 differential proteins, 25 were localized in the cytoplasm, 16 were localized in the extracellular matrix, 16 were localized in the nucleus, five were localized in the mitochondria, two were localized in both the nucleus and cytoplasm, two were localized in the plasma membrane, and the remaining three were localized in the endoplasmic reticulum, cytoskeleton, and peroxisome, respectively. As shown in Fig. 4e, we also analyzed the clusters of orthologous groups of differentially expressed proteins. There were two RNA processing and modification proteins; two chromatin structure and dynamics proteins; five energy production and conversion proteins; one cell cycle control protein; one cell division and chromosome partitioning protein; one translation protein; one ribosomal structure and biogenesis protein; two transcription proteins; two replication, recombination, and repair proteins; one cell wall/membrane/envelope biogenesis protein; three post-translational modification, protein turnover, and chaperone proteins; two signal transduction mechanisms proteins; one intracellular trafficking, secretion, and vesicular transport protein; five cytoskeleton proteins; nine general function prediction proteins; and two unknown function proteins.

Functional enrichment of differentially expressed proteins in the Hst/T1DM groups

Based on functional annotations, we carried out functional enrichment analysis using GO and KEGG analyses to clarify changes in the differentially expressed proteins. As shown in Fig. 5a, differentially expressed proteins were mainly involved in leukocyte aggregation, leukocyte cell-cell adhesion, oxygen transport, gas transport, isoprenoid biosynthetic process, cardiac muscle adaptation, striated muscle adaptation, muscle hypertrophy in response to stress, positive regulation of hemostasis, and positive regulation of coagulation in BPs. For CCs, most proteins were MHC protein complexes, MHC class I protein complexes, hemoglobin complexes, and nucleosomes. Similarly, the differentially expressed proteins were involved in MFs, including Toll-like receptor 4 binding, Toll-like receptor binding, RAGE receptor binding, arachidonic acid binding, fatty acid derivative binding, long-chain fatty acid binding, fatty acid binding, oxygen transporter activity, oxygen binding, icosatetraenoic acid binding, and icosanoid binding.

The results of KEGG pathway enrichment analysis (Fig. 5b) revealed that most of the proteins were enriched in type I diabetes mellitus, viral myocarditis, cell adhesion molecules, antigen processing and presentation, and the interleukin (IL)-17 signaling pathway.

Protein-protein interaction network

The overlapping differentially expressed proteins of the T1DM/control and Hst/T1DM groups were imported into STRING for visualization of the protein-protein interaction network (Fig. 6).

Verification of candidate proteins differentially expressed in the coronary artery

We verified the abundance of the proteins KNG1, S100A9, and S100A8 in coronary arteries from each group using western blotting. Consistent with the proteomics data, all three proteins were notably

upregulated in the T1DM group compared to that in the control group and were significantly downregulated in the Hst group compared to that in the T1DM group ($P < 0.05$ or $P < 0.01$; Fig. 7).

Discussion

STZ is widely used to induce diabetes in animal models and can be taken up by pancreatic β-cells. β-Cell death is induced by excessive production of reactive oxygen species, resulting in diabetic symptoms such as hyperglycemia and impaired glucose tolerance [22]. Hst can reduce blood glucose levels and blood lipids by promoting insulin secretion, positively regulating the disordered carbohydrate metabolic enzymes, and reducing the levels of liver and kidney injury markers in STZ-induced experimental rats [13]. Moreover, Hst also reduces oxidative stress caused by hyperglycemia in the pancreas and prevents toxicity induced by STZ [13]. Orallo *et al.* [23] confirmed that Hst may have significant effects on vascular relaxation in rat aortic smooth muscle by increasing the intracellular concentrations of cAMP and cGMP. Although many cardiovascular protective mechanisms of Hst have been widely reported, few studies have been conducted on diabetes-related cardiovascular diseases. Therefore, we used STZ to induce T1DM in a rat model, observed changes in the coronary artery in rats, and used proteomics-based methods to study the cardiovascular protective effects of Hst.

Our experimental results showed that Hst lowered blood glucose and ameliorated coronary artery injury in T1DM model rats. The proteomic results revealed that some of the differentially expressed proteins after Hst intervention were involved in leukocyte aggregation and leukocyte cell-cell adhesion processes in the BP category and that most of these differentially expressed proteins possessed MFs related to binding. In our subsequent analyses, we focused on the roles of S100A8, S100A9, and KNG1.

Previous studies have shown an association between chronic inflammation and the presence of cardiovascular complications in individuals with type 1 diabetes [24]. S100A8 and S100A9, members of the alarmin family and S100 family of calcium-modulated proteins, are expressed in cells of myeloid origin, particularly in monocytes and neutrophils, and have been linked with cardiovascular disease [25–27]. Weak expression has also been observed in vascular endothelial cells [28, 29] and platelets [30]. S100A8 and S100A9 generally exist as homodimers, but preferentially form the S100A8/A9 heterodimer in the presence of $Zn^{2+}$and Ca^{2+}[31], which is an active mediator in the pathogenesis of various autoimmune and inflammatory conditions [32, 33]. Damage-associated molecular patterns (DAMPs) are endogenous pro-inflammatory molecules that activate innate immunity pathways and are involved in cellular functions under normal homeostasis; these molecules are released after cell death, signaling tissue damage [34, 35]. S100A8 andS100A9 have been identified as DAMPs that can bind to cell surface receptors, such as Toll-like receptor 4 and receptor for advanced glycation end products (RAGE) [30], leading to a pro-inflammatory cascade and accelerating the chronic inflammatory process of atherogenesis associated with diabetes [31]. Additionally, studies in animal models have demonstrated that the S100A8/A9 complex is crucial for the generation of atherosclerosis and vascular injury [36]. S100A8/A9 binds heparan sulfate proteoglycans and carboxylated glycans on endothelial cells [37, 38] and triggers endothelial activation, characterized by the enhanced production of inflammatory cytokines

and chemokines [39, 40], increased expression of adhesion molecules [39, 40], and increased platelet aggregation at the surface of the endothelium [39]. The overexpression of vascular adhesion molecules on endothelial cells enhances the invasion of monocytes into the vascular wall and eventually leads to the formation of atherosclerosis and cardiovascular disease [41]. Furthermore, endothelial cells treated with S100A8/A9 show downregulation of anti-apoptotic genes and genes responsible for the integrity of the endovascular monolayer [39, 42]. Extended S100A8/A9 exposure leads to endothelial cell dysfunction and increased endothelial permeability [42]. These effects are partly mediated by RAGE [43] and exacerbated by hyperglycemia [40, 44]. Two other studies have supported the use of S100A8/A9 as a predictor of initial [45] or recurrent cardiovascular events [46]. Our results showed that the expression levels of S100A8 and S100A9 in the coronary arteries of T1DM rats were significantly higher than those in the control group. After Hst intervention, the expression levels of S100A8 and S100A9 were significantly decreased. In addition, enrichment in the IL-17 pathway was detected. Therefore, we speculated that S100A8 and S100A9 may be involved in the pathogenesis of T1DM vascular disease by promoting an inflammatory response and affecting endothelial function; Hst downregulated S100A8 and S100A9 to mediate these effects.

Kininogens (KNGs) are multifunctional proteins involved in multiple pathways. These proteins participate in the generation of kinins, act as cofactors for the intrinsic coagulation system, inhibit cysteine proteases, and modulate platelet aggregation, angiogenesis, and the acute-phase response. KNG1, mainly produced by hepatocytes, is a macromolecular substance that is a crucial component of the kallikrein system. KNGs produce high- and low-molecular-weight KNGs under the action of kallikrein [47]. KNG1 is the precursor of the kallikrein-kinin system and acts as a starting substrate for clinical research [48]. Recent proteomic analysis of the aorta and kidney in T1DM model rats showed that diabetes induced KNG1 expression, and this mechanism was regulated by hyperglycemia. Additionally, insulin can reverse KNG expression by controlling blood glucose levels [49]. Our results also show an increase in KNG1 levels in the T1DM coronary arteries. Notably, the *KNG1* gene was identified as a positional candidate gene for internal elastic lamina lesions (a new event of atherosclerosis) [50], and high levels of KNG were detected in patients with in-stent restenosis after angioplasty, indicating that these patients may exhibit increased basal activity of kinins supportive of a pro-inflammatory and atherogenic state [51]. Additional evidence demonstrates the contribution of the *KNG1* gene to adiponectin levels and hypertension [52, 53], which are well-established risk factors for atherosclerosis. In addition, studies conducted in animal models have shown that KNG1 inhibition can prevent cardiovascular diseases (such as myocardial infarction) by combining antithrombotic and anti-inflammatory mechanisms [54]. KNG1 is also an essential physiological and pathological factor involved in regulating blood pressure, inflammation, and cardiac function [55]; however, its role in diabetes-related cardiovascular disease is unclear. In this study, we found that KNG1 expression was increased in the coronary arteries of T1DM model rats and that Hst treatment decreased KNG1 expression. Thus, KNG1 may be associated with T1DM-related cardiovascular injury, and Hst may block vascular damage by downregulating KNG1.

we found that S100A8, S100A9, and KNG1 were involved in mediating the protective effects of Hst on coronary artery injury in T1DM model rats. However, there were limitations to this study. For example,

because the coronary artery samples were small, we used mixtures of samples from each group for the experiments and detected changes in protein expression. The observed changes therefore could not be attributed to specific rats. Therefore, further proteomic analyses of heart tissues are needed. Additionally, pharmacokinetic changes may occur after oral administration of Hst, and it is also necessary to study the metabolites of Hst. With the development of genomic, proteomic, transcriptomic, and metabolomic tools, further systematic analyses of the roles of Hst will be possible.

Conclusions

In this study, TMT quantitative proteomics was used to interpret the protective mechanism of hesperetin on coronary artery injury in rats with diabetes mellitus. We found that hesperetin can improve the weight loss and blood glucose increase of diabetes, and preliminarily found several proteins S100A8, S100A9 and KNG1 involved in the protective mechanism of hesperetin, which may be involved in the inflammatory process in the development of diabetes.

Abbreviations

T1DM, type 1 diabetes mellitus; Hst, hesperetin; HE, hematoxylin and eosin; STZ, streptozotocin; SD, Sprague-Dawley; HPLC, high-performance liquid chromatography; LC-MS/MS, liquid chromatography-tandem mass spectrometry; GO, Gene Ontology; KEGG, Kyoto Encyclopedia of Genes and Genomes

Declarations

Acknowledgments

The authors thank Jingjie PTM BIO (Hangzhou, China) for assistance with mass spectrometry analysis.

Authors' contributions

XGF and HPT prepared the first draft. ZXY was responsible for data sorting. CZY and WL, was responsible for revising the manuscript. LY was responsible for text editing and submission. All authors agreed to this information before submission.

Funding

This work was supported by the Youth Science Foundation of the National Natural Science Foundation of China (grant no.: 81603111).

Availability of data and materials

The datasets used and/or analyzed during the current study are available from

the corresponding author on reasonable request.

Ethics approval and consent to participate

All animal experiments have been approved by the Ethics Committee of Shanxi Medical University, and all procedures are carried out in accordance with the guidelines of the Ethics Committee.

Consent for publication

The manuscript is approved by all authors for publication.

Competing interests

The authors declare that they have no competing interests.

Author details

[1]Department of Pharmacology, Shanxi Medical University, Taiyuan, China.[2]Labratory Animal Center, Shanxi Medical University, Taiyuan, China.[3]General Medical Department, Shanxi Bethune Hospital, Taiyuan, China.

References

1. Saeedi P, Petersohn I, Salpea P, et al. Global and regional diabetes prevalence estimates for 2019 and projections for 2030 and 2045: Results from the International Diabetes Federation Diabetes Atlas, 9 edition. Diabetes Res Clin Pract. 2019;157:107843.
2. Krolewski AS, Kosinski EJ, Warram JH, et al. Magnitude and determinants of coronary artery disease in juvenile-onset, insulin-dependent diabetes mellitus. Am J Cardiol. 1987;59(8):750–5.
3. Deckert T, Poulsen JE, Larsen M. Prognosis of diabetics with diabetes onset before the age of thirty-one. I. Survival, causes of death, and complications. Diabetologia. 1978;14(6):363–70.
4. Dorman JS, Laporte RE, Kuller LH, et al. The Pittsburgh insulin-dependent diabetes mellitus (IDDM) morbidity and mortality study. Mortality results. Diabetes. 1984;33(3):271–6.
5. Orchard TJ, Costacou T, Kretowski A, et al. Type 1 diabetes and coronary artery disease. Diabetes Care. 2006;29(11):2528–38.
6. Soedamah-Muthu SS, Fuller JH, Mulnier HE, et al. All-cause mortality rates in patients with type 1 diabetes mellitus compared with a non-diabetic population from the UK general practice research database, 1992–1999. Diabetologia. 2006;49(4):660–6.
7. Rhee SY, Kim YS. The Role of Advanced Glycation End Products in Diabetic Vascular Complications. Diabetes Metab J. 2018;42(3):188–95.
8. Donaghue K, Jeanne Wong SL. Traditional Cardiovascular Risk Factors in Adolescents with Type 1 Diabetes Mellitus. Curr Diabetes Rev. 2017;13(6):533–43.
9. Ferreira I, Hovind P, Schalkwijk CG, et al. Biomarkers of inflammation and endothelial dysfunction as predictors of pulse pressure and incident hypertension in type 1 diabetes: a 20 year life-course study

in an inception cohort. Diabetologia. 2018;61(1):231–41.

10. Domingueti CP, Dusse LMSA, Carvalho MdG, et al. Diabetes mellitus: The linkage between oxidative stress, inflammation, hypercoagulability and vascular complications. J Diabetes Complications. 2016;30(4):738–45.
11. Yaribeygi H, Atkin SL, Sahebkar A. A review of the molecular mechanisms of hyperglycemia-induced free radical generation leading to oxidative stress. Journal of cellular physiology. 2019;234(2):1300–12.
12. Schofield J, Ho J, Soran H. Cardiovascular Risk in Type 1 Diabetes Mellitus. Diabetes Ther. 2019;10(3):773–89.
13. Jayaraman R, Subramani S, Sheik Abdullah SH, et al. Antihyperglycemic effect of hesperetin, a citrus flavonoid, extenuates hyperglycemia and exploring the potential role in antioxidant and antihyperlipidemic in streptozotocin-induced diabetic rats. Biomed Pharmacother. 2018;97:98–106.
14. Sharma M, Akhtar N, Sambhav K, et al. Emerging potential of citrus flavanones as an antioxidant in diabetes and its complications. Curr Top Med Chem. 2015;15(2):187–95.
15. Yang Z, Liu Y, Deng W, et al. Hesperetin attenuates mitochondria-dependent apoptosis in lipopolysaccharide-induced H9C2 cardiomyocytes. Mol Med Rep. 2014;9(5):1941–6.
16. Sugasawa N, Katagi A, Kurobe H, et al. Inhibition of Atherosclerotic Plaque Development by Oral Administration of α-Glucosyl Hesperidin and Water-Dispersible Hesperetin in Apolipoprotein E Knockout Mice. J Am Coll Nutr. 2019;38(1):15–22.
17. Parhiz H, Roohbakhsh A, Soltani F, et al. Antioxidant and anti-inflammatory properties of the citrus flavonoids hesperidin and hesperetin: an updated review of their molecular mechanisms and experimental models. Phytother Res. 2015;29(3):323–31.
18. Hertog MGL, Feskens EJM, Kromhout D, et al. Dietary antioxidant flavonoids and risk of coronary heart disease: the Zutphen Elderly Study. Lancet. 1993;342(8878):1007–11.
19. Geleijnse JM, Launer LJ, Kuip DAM, Van Der, et al. Inverse association of tea and flavonoid intakes with incident myocardial infarction: the Rotterdam Study. Am J Clin Nutr. 2002;75(5):880–6.
20. Yu L, Longgang N, Lijuan C, et al. Hesperetin inhibits rat coronary constriction by inhibiting Ca(2+) influx and enhancing voltage-gated K(+) channel currents of the myocytes. Eur J Pharmacol. 2014;735(1):193–201.
21. Yong-Ri J, Xiang-Hua H, Yong-He Z, et al. Antiplatelet activity of hesperetin, a bioflavonoid, is mainly mediated by inhibition of PLC-gamma2 phosphorylation and cyclooxygenase-1 activity. Atherosclerosis. 2007;194(1):144–52.
22. Lukić ML, Stosić-Grujicić S, Shahin A. Effector mechanisms in low-dose streptozotocin-induced diabetes. Dev Immunol. 1998;6(1–2):119–28.
23. Orallo F, Alvarez E, Basaran H, et al. Comparative study of the vasorelaxant activity, superoxide-scavenging ability and cyclic nucleotide phosphodiesterase-inhibitory effects of hesperetin and hesperidin. Naunyn Schmiedebergs Arch Pharmacol. 2004;370(6):452–63.

24. Schram MT, Chaturvedi N, Schalkwijk CG, et al. Markers of inflammation are cross-sectionally associated with microvascular complications and cardiovascular disease in type 1 diabetes–the EURODIAB Prospective Complications Study. Diabetologia. 2005;48(2):370–8.
25. Hessian PA, Edgeworth J, Hogg N. MRP-8 and MRP-14, two abundant Ca(2+)-binding proteins of neutrophils and monocytes. J Leukoc Biol. 1993;53(2):197–204.
26. Averill MM, Kerkhoff C, Bornfeldt KE. S100A8 and S100A9 in cardiovascular biology and disease. Arterioscler Thromb Vasc Biol. 2012;32(2):223–9.
27. Jesse G, Xing YW, Eric Y, et al. Pleiotropic roles of S100A12 in coronary atherosclerotic plaque formation and rupture. J Immunol. 2009;183(1):593–603.
28. Frosch M, Strey A, Vogl T, et al. Myeloid-related proteins 8 and 14 are specifically secreted during interaction of phagocytes and activated endothelium and are useful markers for monitoring disease activity in pauciarticular-onset juvenile rheumatoid arthritis. Arthritis Rheum. 2010;43(3):628–37.
29. Yen T, Harrison CA, Devery JM, et al. Induction of the S100 chemotactic protein, CP-10, in murine microvascular endothelial cells by proinflammatory stimuli. Blood. 1997;90(12):4812–21.
30. Pruenster M, Vogl T, Roth J, et al. S100A8/A9: From basic science to clinical application. Pharmacol Ther. 2016;167:120–31.
31. Alexandru S, Cotoi OS. S100A8 and S100A9: DAMPs at the crossroads between innate immunity, traditional risk factors, and cardiovascular disease. Mediators Inflamm. 2013;2013(3):828354.
32. Nacken W, Roth J, Sorg C, et al. S100A9/S100A8: Myeloid representatives of the S100 protein family as prominent players in innate immunity. Microsc Res Tech. 2003;60(6):569–80.
33. Ehrchen JM, Cord S, Dirk F, et al. The endogenous Toll-like receptor 4 agonist S100A8/S100A9 (calprotectin) as innate amplifier of infection, autoimmunity, and cancer. J Leukoc Biol. 2009;86(3):557–66.
34. Kim N, Dixit VM. Signaling in innate immunity and inflammation. Cold Spring Harb Perspect Biol. 2012;4(3):829–41.
35. Chan JK, Roth J, Oppenheim JJ, et al. Alarmins: awaiting a clinical response. J Clin Invest. 2012;122(8):2711–9.
36. Kevin C, Huiyun G, Yunmei W, et al. Myeloid-related protein-8/14 is critical for the biological response to vascular injury. Circulation. 2009;120(5):427–36.
37. Robinson MJ, Philippe T, Richard P, et al. The S100 family heterodimer, MRP-8/14, binds with high affinity to heparin and heparan sulfate glycosaminoglycans on endothelial cells2002;277(5):3658–3665.
38. Srikrishna G, Panneerselvam K, Westphal V, et al. Two proteins modulating transendothelial migration of leukocytes recognize novel carboxylated glycans on endothelial cells. J Immunol. 2001;166(7):4678–88.
39. Dorothee V, Anke S, Annette J, et al. Myeloid-related proteins 8 and 14 induce a specific inflammatory response in human microvascular endothelial cells. Blood. 2005;105(7):2955–62.

40. Ehlermann P, Eggers K, Bierhaus A, et al. Increased proinflammatory endothelial response to S100A8/A9 after preactivation through advanced glycation end products. Cardiovasc Diabetol. 2006;5:6.
41. Ross R. Atherosclerosis–an inflammatory disease. N Engl J Med. 1999;340(2):115–26.
42. Dorothee V, Katarzyna B, Thomas V, et al. MRP8/MRP14 impairs endothelial integrity and induces a caspase-dependent and -independent cell death program. Blood. 2007;109(6):2453–60.
43. Evis H, De-Xiu B, Hudson BI, et al. Vascular and inflammatory stresses mediate atherosclerosis via RAGE and its ligands in apoE-/- mice. J Clin Invest. 2008;118(1):183–94.
44. Stocca A, O'Toole D, Hynes N, et al. A Role for MRP8 in in stent restenosis in diabetes. Atherosclerosis. 2012;221(2):325–32.
45. Healy AM, Pickard MD, Pradhan AD, et al. Platelet expression profiling and clinical validation of myeloid-related protein-14 as a novel determinant of cardiovascular events. Circulation. 2006;113(19):2278–84.
46. Morrow DA, Yunmei W, Kevin C, et al. Myeloid-related protein 8/14 and the risk of cardiovascular death or myocardial infarction after an acute coronary syndrome in the Pravastatin or Atorvastatin Evaluation and Infection Therapy: Thrombolysis in Myocardial Infarction (PROVE IT-TIMI 22) trial. Am Heart J. 2008;155(1):49–55.
47. Masao K, Oliver S. The kallikrein-kinin system in health and in diseases of the kidney. Kidney Int. 2009;75(10):1019–30.
48. Sharma JN, Narayanan P. The Kallikrein–Kinin Pathways in Hypertension and Diabetes. Prog Drug Res. 2014;69:15–36.
49. Al HM, Elmedawar M, Zhu R, et al. Proteome profiling in the aorta and kidney of type 1 diabetic rats. PLoS One. 2017;12(11):e0187752.
50. Stoll M, Cowley AW, Tonellato PJ, et al. A genomic-systems biology map for cardiovascular function. Science. 2001;294(5547):1723–6.
51. Ribeiro MS, Dellalibera-Joviliano R, Becari C, et al. Characterization of the Kallikrein-kinin System, Metalloproteinases, and Their Tissue Inhibitors in the In-stent Restenosis after Peripheral Percutaneous Angioplasty. Ann Vasc Surg. 2014;28(4):1005–15.
52. Ying W, Yun L, Lange EM, et al. Genome-wide association study for adiponectin levels in Filipino women identifies CDH13 and a novel uncommon haplotype at KNG1-ADIPOQ. Hum Mol Genet. 2010;19(24):4955–64.
53. Weiyan Z, Yaping W, Laiyuan W, et al. Gender-specific association between the kininogen 1 gene variants and essential hypertension in Chinese Han population. J Hypertens. 2009;27(3):484–90.
54. Friederike L, Eva G, Peter K, et al. Kininogen deficiency protects from ischemic neurodegeneration in mice by reducing thrombosis, blood-brain barrier damage, and inflammation. Blood. 2012;120(19):4082–92.

55. Gonzalezcalero L, Martinlorenzo M, Ramosbarron A, et al. Urinary Kininogen-1 and Retinol binding protein-4 respond to Acute Kidney Injury: predictors of patient prognosis? Sci Rep. 2016;6(1):19667.

Figures

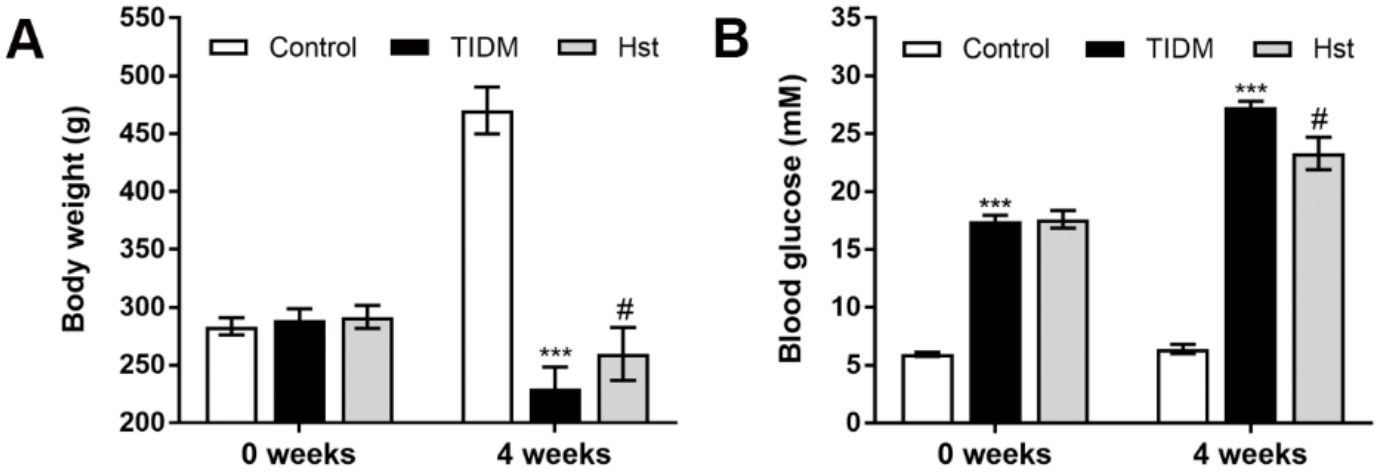

Figure 1

Effects of Hst on body weight (A) and blood glucose (B). Data are expressed as means ± standard deviations (n = 14–15/group). ***P < 0.001 versus the control group, #P < 0.05 versus the T1DM group.

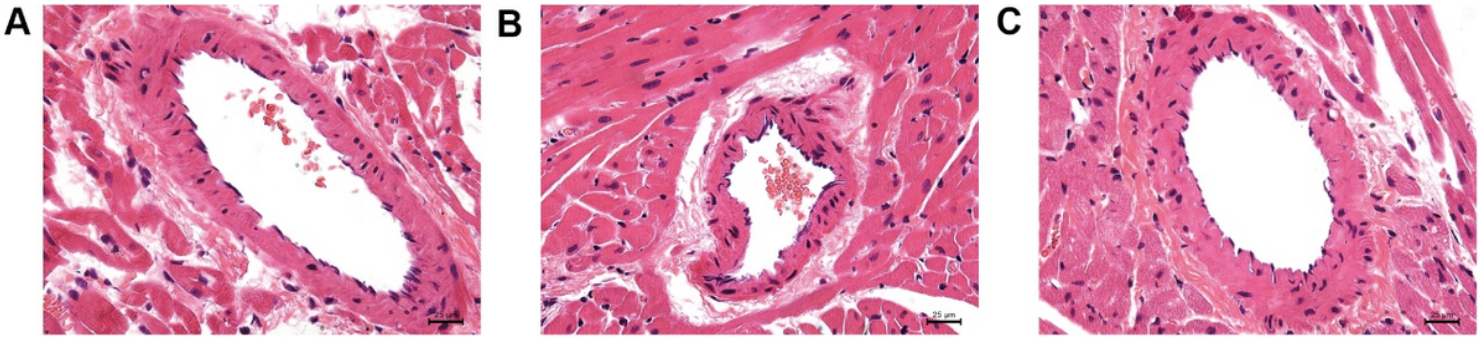

Figure 2

Histomorphological comparison of coronary arteries in rats for each group (HE staining, 400×). (A-C): Control, T1DM, and Hst groups.

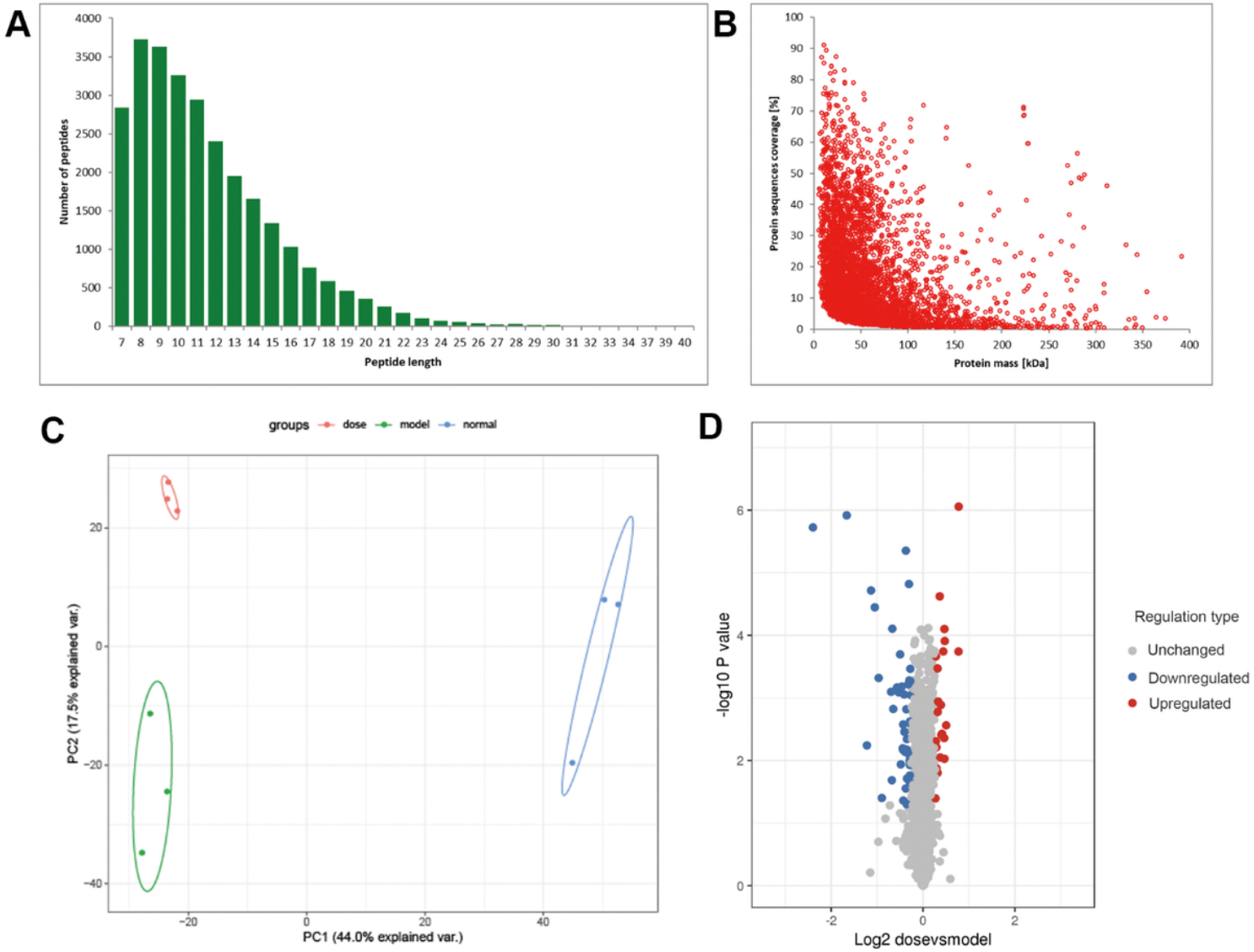

Figure 3

Differentially expressed proteins were evaluated using TMT proteomics. (A) Length distribution of the peptides identified using mass spectrometry. (B) Relationship between protein molecular weight and coverage. (C) Evaluation of protein quantitative repeatability using principal component analysis (PCA) statistical analysis. (D) Volcano plot of differentially expressed proteins in Hst/T1DM. Red dots represent upregulated proteins, blue dots represent downregulated proteins, and gray dots represent proteins with no significant differences. The horizontal axis is the ratio of protein expression after log2 conversion. The vertical axis is p value from significance tests converted using -log10. After Hst treatment, there were 47 upregulated and 22 downregulated proteins.

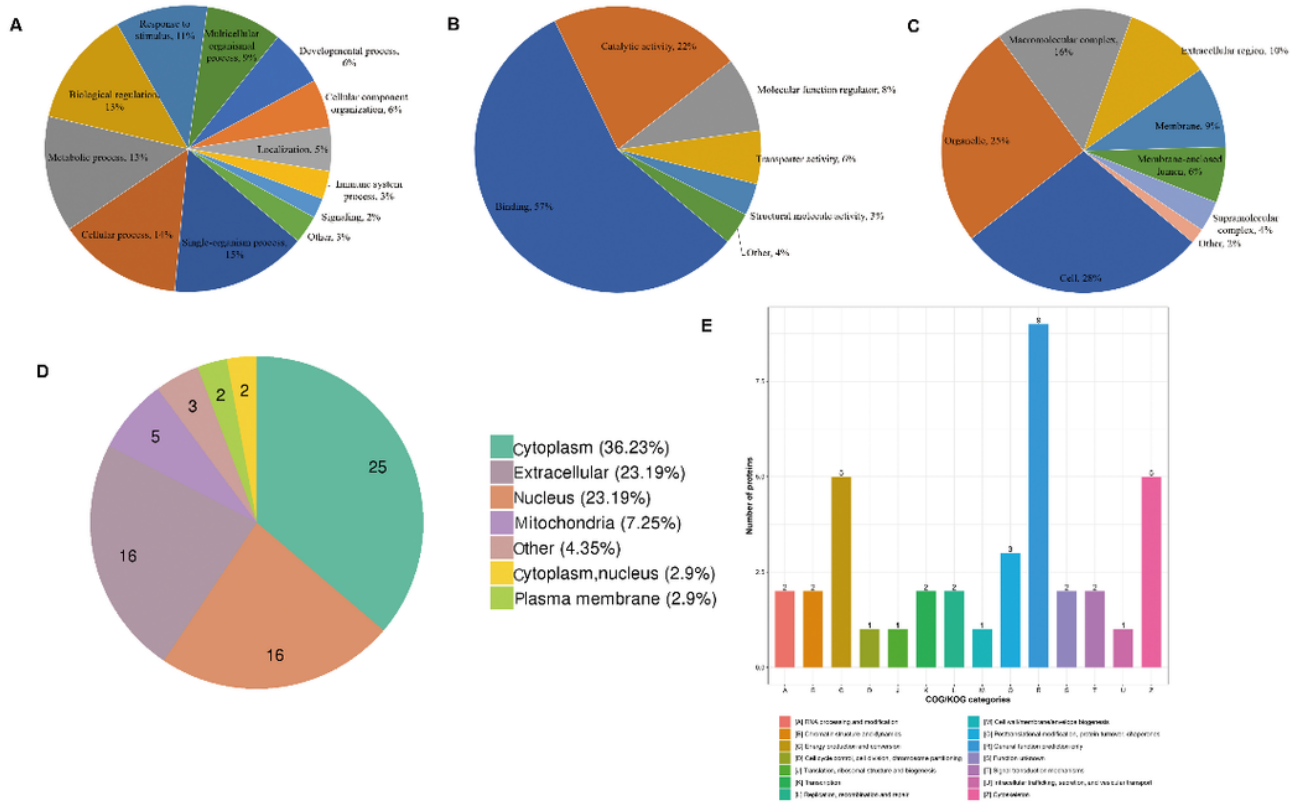

Figure 4

Functional classification of differentially expressed proteins in the Hst/TIDM group. (A) Biological processes (BPs). (B) Molecular functions (MFs). (C) Cellular components (CCs). (D) Subcellular localization. (E) Clusters of orthologous groups of proteins.

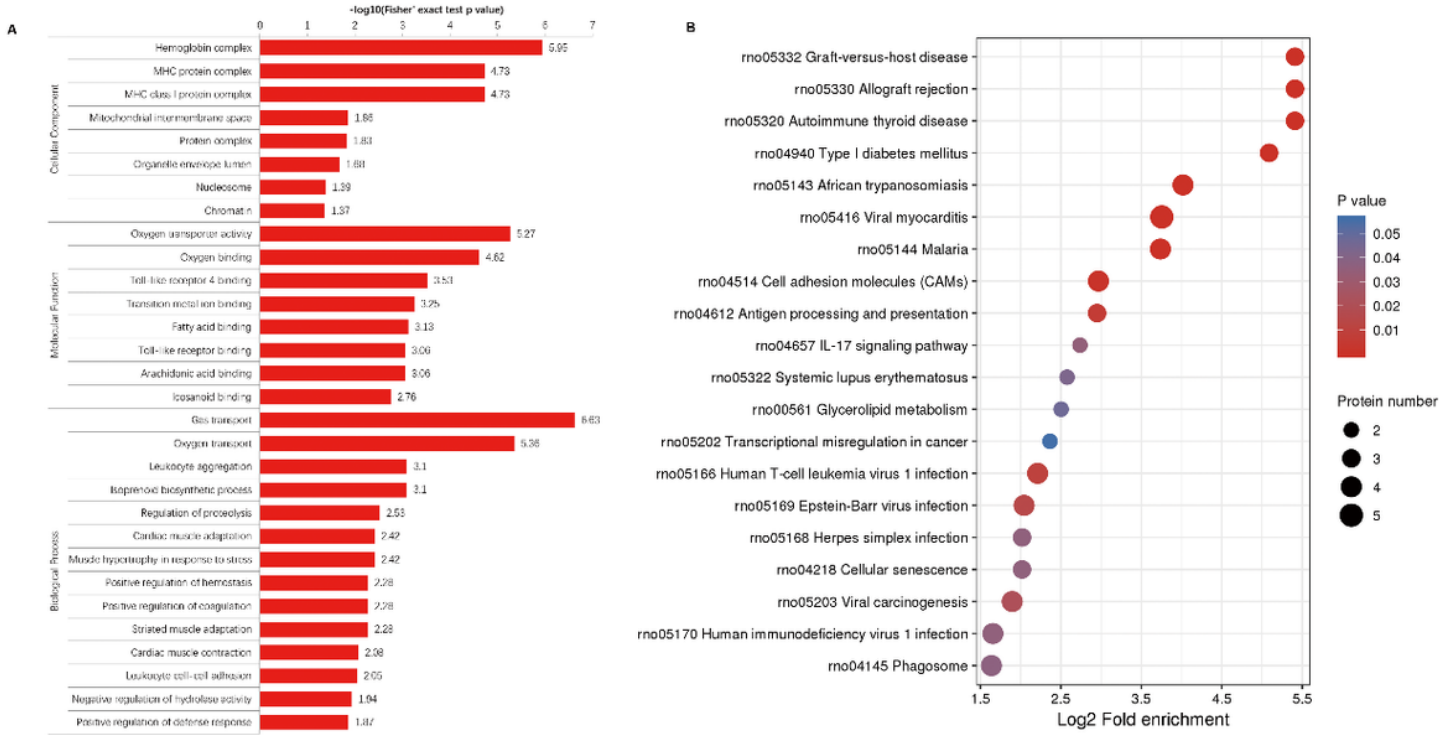

Figure 5

Functional enrichment of differentially expressed proteins in the Hst/TIDM group. (A) Bar diagram of GO (BP, MF, CC) enrichment. The vertical axis is the GO classification, and the horizontal axis is the Fisher exact test value after logarithmic conversion. The longer the bar chart, the more significant the enrichment of differentially expressed proteins in this classification or function. (B) Bubble diagram of KEGG enrichment. The vertical axis of the bubble diagram represents the pathway, and the horizontal axis represents the log2 conversion value of the proportion of differential expressed proteins to the class identification proteins in this pathway. The circle color represents the enriched P value, and the circle size indicates the number of differentially expressed proteins in the pathway.

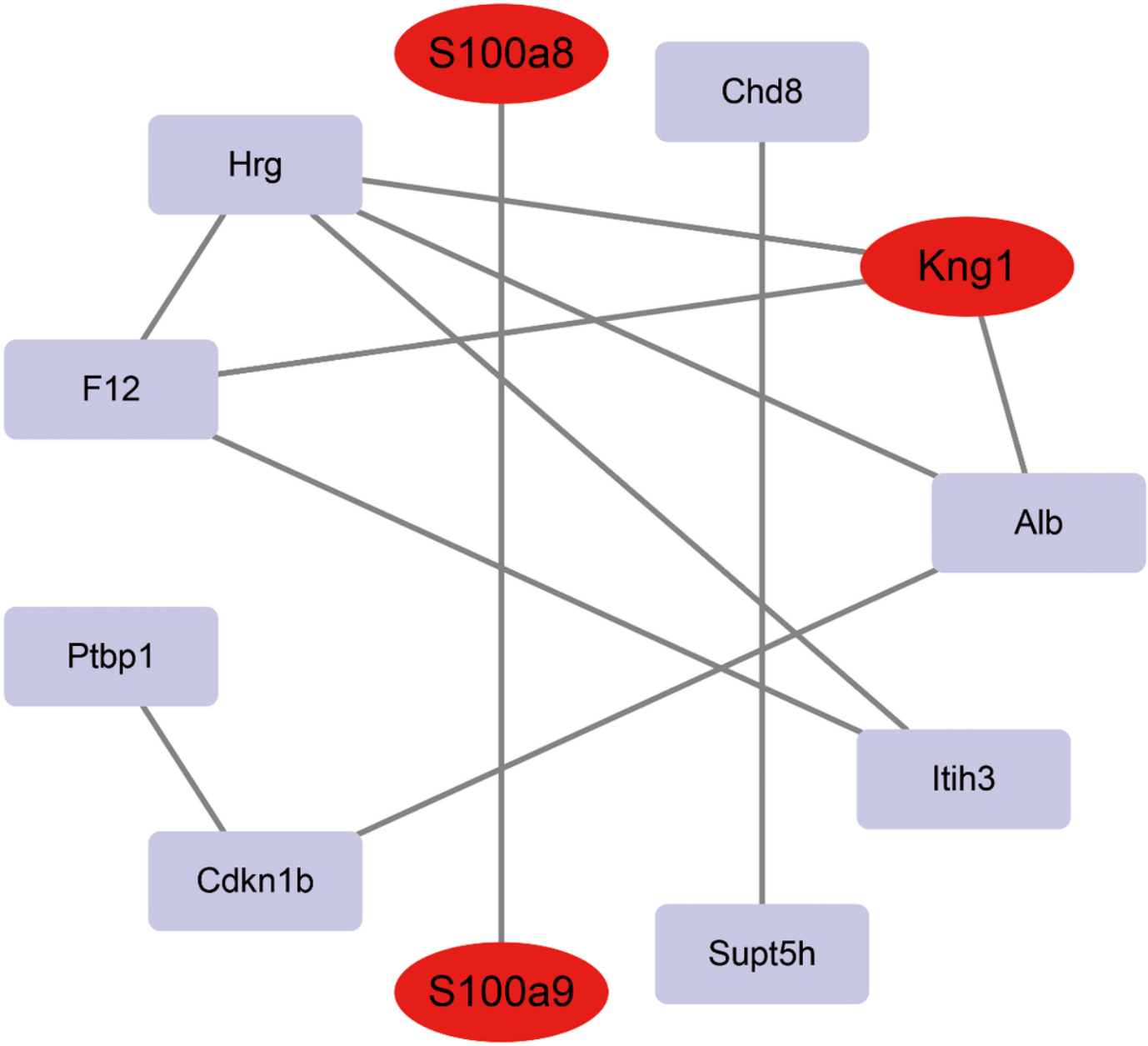

Figure 6

The protein-protein interaction network of the overlapping differentially expressed proteins in the T1DM/control and Hst/T1DM groups.

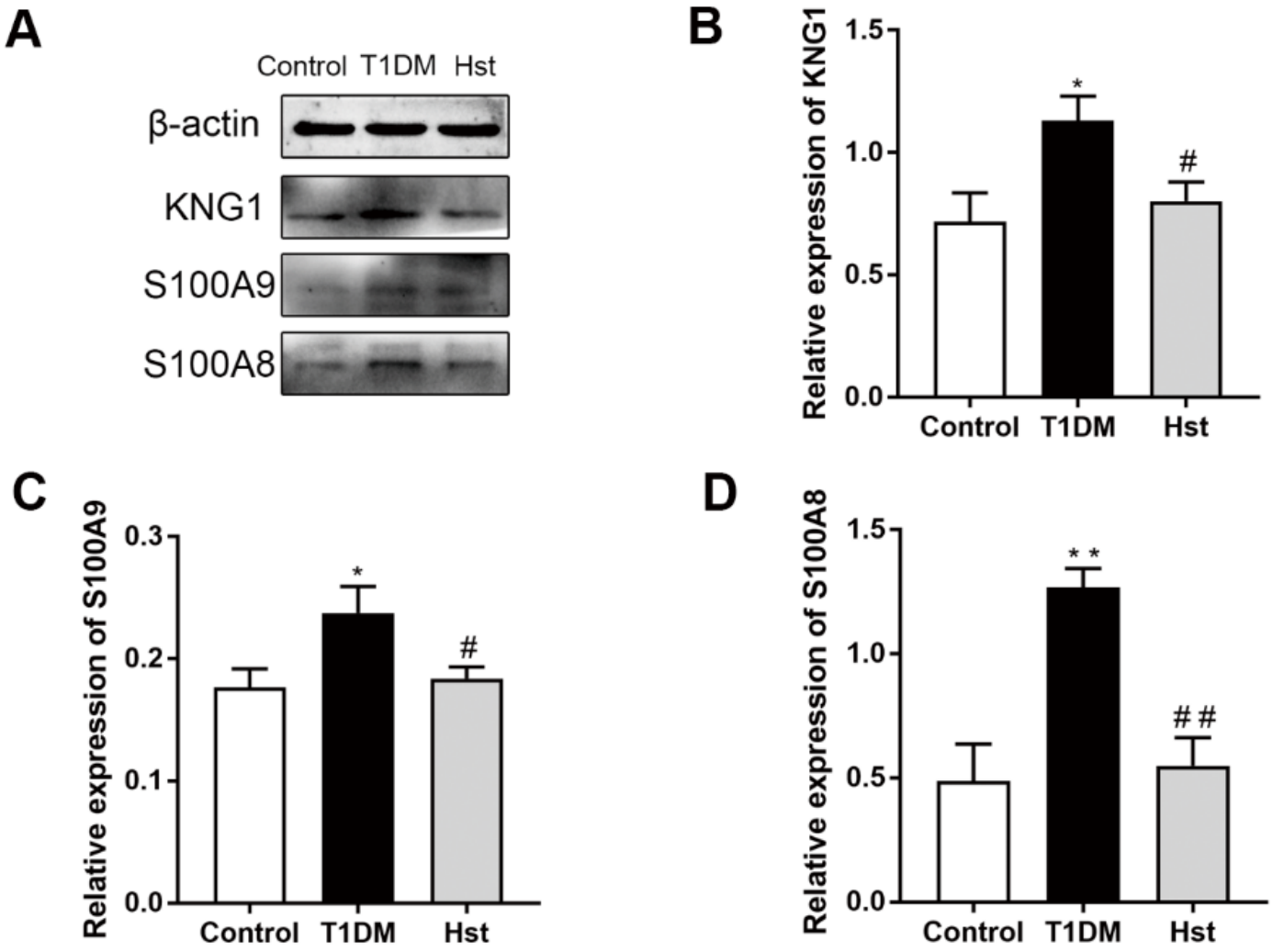

Figure 7

Validation of differentially expressed proteins in the control, T1DM, and Hst groups using western blotting. (A) Representative western blots. (B–D) Protein expression levels of KNG1, S100a9, and S100a8. Data are represented as means ± standard deviations (n = 3). T1DM versus control: *P < 0.05, **P < 0.01; Hst versus T1DM: #P < 0.05, ##P < 0.01.